American Mineralogist, Volume 87, pages 501–513, 2002

The role of Fe and cation order in the crystal chemistry of surinamite, $(Mg,Fe^{2+})_3(Al,Fe^{3+})_3O[AlBeSi_3O_{15}]$: A crystal structure, Mössbauer spectroscopic, and optical spectroscopic study

JACQUES BARBIER,[1,*] EDWARD S. GREW,[2] ELKE HÅLENIUS,[3] ULF HÅLENIUS,[4] AND MARTIN G. YATES[2]

[1]Department of Chemistry, McMaster University, Hamilton, Ontario L8S 4M1, Canada
[2]Department of Geological Sciences, University of Maine, 5790 Bryand Center, Orono, Maine 04469, U.S.A.
[3]SGAB Analytica, Box 511, SE-183 25 Täby, Sweden
[4]Department of Mineralogy, Swedish Museum of Natural History, Box 50007, SE-104 05 Stockholm, Sweden

ABSTRACT

The crystal structure of surinamite from "Christmas Point," Enderby Land, Antarctica, has been newly refined by single-crystal X-ray diffraction: $^{VI}(Mg_{2.26}Fe^{2+}_{0.74}Fe^{3+}_{0.39}Al_{2.61})O^{IV}(Al_{1.00}Be_{1.00}Si_{3.00})O_{15}$ (simplified formula), space group $P2/n$, $a = 9.915(2)$, $b = 11.368(2)$, $c = 9.617(2)$, b = 109.30(2)°, $Z = 4$, $wR(F^2) = 0.074$ for 4876 independent reflections. The refined site occupancies agree well with the chemical composition determined by electron microprobe analysis and with the Fe^{3+}/Fe^{2+} ratio estimated from stoichiometry. The surinamite structure is characterized by an ordered Al/Be/Si distribution on the tetrahedral sites and by charge ordering with extensive Mg^{2+}-Fe^{2+} and Al^{3+}-Fe^{3+} exchange on the octahedral sites. This cation ordering is distinct from that observed in related phases of the sapphirine series and aenigmatite groups, and the difference is linked to the unique structural topology of the tetrahedral chains in surinamite. Optical and Mössbauer spectra of surinamite have been fully interpreted in terms of an octahedral distribution of Fe^{2+} and Fe^{3+} cations that agrees very well with the X-ray site populations. Both the X-ray and Mössbauer data establish the absence of significant tetrahedral Fe and the non-uniform distribution of octahedral Fe. Intense and strongly polarized absorption bands caused by IVCT-processes in clusters of Fe^{3+} and Fe^{2+} iron in edge-sharing octahedral sites produce the unusual color and pleochroism observed in surinamite.

INTRODUCTION

Surinamite, $(Mg,Fe^{2+})_3(Al,Fe^{3+})_3O[AlBeSi_3O_{15}]$ is a single-chain silicate found in high-grade metapelites and metapegmatites at seven localities worldwide (Baba et al. 2000). It closely resembles sapphirine in structure (Moore and Araki 1983) and has the same dominantly blue coloration as this mineral, but its colors are distinctive with greenish and purplish hues far more pronounced than in sapphirine (e.g., de Roever et al. 1976; this paper, Fig. 1); the purple being reminiscent of color seen in alkali amphibole. These colors suggest a major role for Fe^{3+} in surinamite crystal chemistry, which is also indicated by stoichiometric formula calculations of surinamite from relatively oxidized rocks (e.g., Grew et al. 2000).

The original structure determination of natural surinamite (Moore and Araki 1983) revealed the major features of its crystal structure, including the close relationship with sapphirine, and confirmed the crystal-chemical role of Be. The latter had been identified as an essential element in surinamite during previous synthetic work in the Mg-Fe-Al-Be-Si-O-H system (de Roever et al. 1981), and later in the Mg-Al-Be-Si-O system (Hölscher et al. 1986). More recently, Be-free germanate analogs of surinamite have been synthesized in the Mg-Al-Ge-O and Mg-Ga-Ge-O systems (Barbier 1996). The structure determination of the gallo-germanate analog, $(Mg_4Ga_2)O[Ga_2Ge_3O_{15}]$, with $C2/c$ symmetry has shown that it corresponds to a new polysomatic variant of the $P2/n$ natural surinamite structure (Barbier 1998). Overall, both the tetrahedral and octahedral cation distributions in surinamite and its synthetic analogs have been found to be more ordered than in the corresponding sapphirine structures. However, the detailed cation ordering in natural surinamite and the Fe^{3+} distribution, in particular, remain to be worked out.

The present paper reports a new crystal-structure refinement, optical spectra, and Mössbauer spectra for surinamite from a metamorphosed pegmatite in Antarctica (Grew et al. 2000). The main objectives of the study are to use new analytical data to resolve several uncertainties in the original structure determination by Moore and Araki (1983), to better establish the extent of cation order in the surinamite structure, and to assess the role of Fe in its crystal chemistry. The cation distribution in surinamite can then be compared with those observed in related minerals, including khmaralite, a partially ordered Be-bearing sapphirine (Barbier et al. 1999).

SAMPLE DESCRIPTION, CHEMISTRY, AND PETROLOGY

Samples 2292C and EG99012207 (shortened to 12207) were collected in 1979 and 1998, respectively, from the "discovery

* E-mail: barbier@mcmaster.ca

0003-004X/02/0004–501$05.00

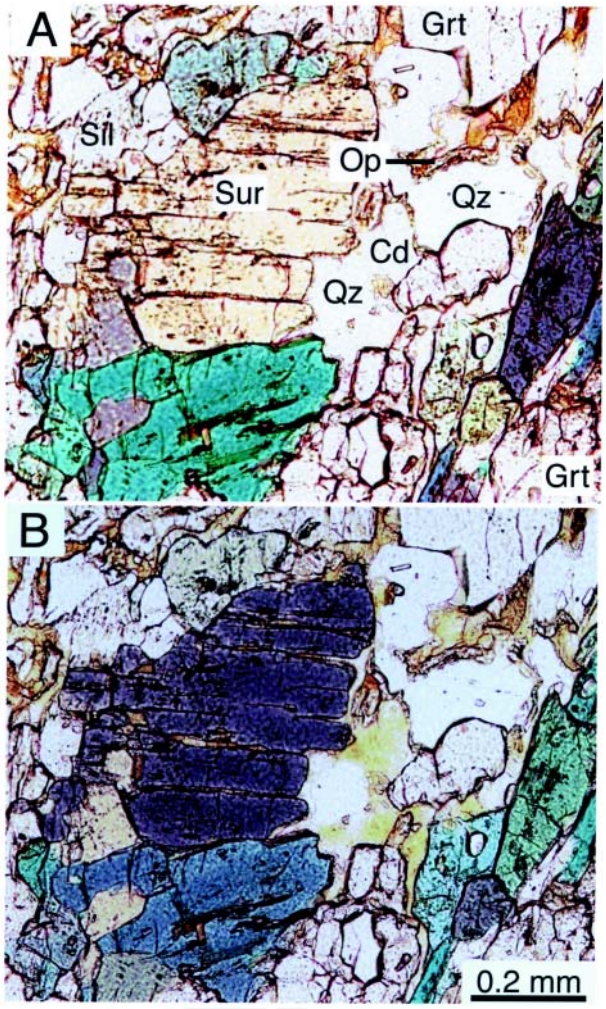

FIGURE 1. Photomicrographs of a surimanite aggregate containing minor quartz (Qz), garnet (Grt, high relief), and sillimanite (Sil) in sample EG88012207 (12207) from "Christmas Point," Khmara Bay, East Antarctica. Orthopyroxene (Op) forms selvages between quartz and biotite (olive brown) and/or cordierite (yellow pleochroism, Cd). Analyzed surinamite grain no. 1 is labeled Sur. A. Grain no. 1 shows the pale yellow-green color characteristic of E||X, whereas the adjacent surinamite grain below it shows a blue-green color close to the one characteristic of E||Z. B. Grain no. 1 shows the purple color characteristic of E||Y.

pegmatite" (no. 1) at "Christmas Point" on an island in Khmara Bay (Casey Bay), East Antarctica (Grew 1981, 1998; Grew et al. 2000). A crystal from sample 2292C was used by Moore and Araki (1983) for their refinement, and, consequently, another crystal from this sample was selected for the present crystal-structure refinement. The amount of material in specimen 2292C was insufficient for Mössbauer spectroscopy, so a sample from a larger specimen was selected for this purpose.

Both samples consist of medium-grained aggregates of surinamite (Fig. 1), sillimanite, quartz, garnet, cordierite, K-feldspar (12207 only), and biotite; sparse orthopyroxene forms selvages between quartz and cordierite or biotite in 12207. Trace amounts of magnetite and hematite, the latter with minor ilmenite exsolution, are present in 2292C, but not in 12207, in which the only Fe-rich accessory mineral is pyrite. The surinamite-bearing aggregates were derived from the breakdown of pegmatitic sapphirine-khmaralite during granulite-facies metamorphism at ~700–900 °C, ~8–9 kbar, when the stable assemblage was quartz + garnet + surinamite + sillimanite (Grew et al. 2000). Partial reaction among these four phases resulted in cordierite and local orthopyroxene during decompression under amphibolite-facies conditions at temperatures below ~700 °C and pressures down to 3 kbar.

The crystal used in the structure refinement and the three grains studied optically, as well as five grains of associated sillimanite, were analyzed in carbon-coated polished thin sections with a wavelength dispersive ARL SEMQ electron microprobe at the University of Maine (15 kV accelerating voltage, 10 nA beam current, and 3 μm spot size). Natural silicates and oxides were used as standards and data were processed with the $\phi(\rho z)$ scheme in which the effect of unanalyzed BeO was included. Except for 2292C, BeO contents were calculated assuming 1Be per 14 cations (Table 1). This assumption is reasonable given the Be content determined by refinement of the crystal structure of no. 2292C and the ion microprobe data on other samples from "Christmas Point" (Grew et al. 2000). $Fe^{3+}/\Sigma Fe$ ratios were calculated in a single step by assuming 11 cations, including Be, and by converting sufficient Fe^{2+} to Fe^{3+} so that the cation charge totaled 32, i.e., enough to balance 16 O atoms. This calculation involves all the analyzed constituents, and thus avoids reliance on a single constituent such as Si, as is the case in other procedures based on stoichiometry. Although the calculation based on total cations may yield a poor approximation of the $Fe^{3+}/\Sigma Fe$ ratio in silicate minerals (e.g., pyroxene, Cawthorn and Collerson 1974), it gave results consistent with the single-crystal and Mössbauer spectroscopic data on surinamite (Table 1). Consequently, we consider it a reasonable procedure for reporting surinamite analyses and for estimating the extent to which Fe is oxidized in surinamite.

Surinamite in 12207 is relatively homogeneous (Table 1); the standard deviations in computing the averages for Si, Al, Fe, and Mg are similar to those for the individual 10-point analyses. The main difference in surinamite composition between the two samples is the Mg/Fe^{2+} ratio if the $Fe^{3+}/\Sigma Fe$ ratios are assumed to be similar. This assumption is reasonable given that the $Fe^{3+}/\Sigma Fe$ ratios determined by crystal structure refinement of 2292C and by Mössbauer spectroscopy of 12207 are nearly identical. In addition, the $Fe^{3+}/\Sigma Fe$ ratios calculated from stoichiometry on both samples are consistent with each other and with the $Fe^{3+}/\Sigma Fe$ ratios determined by these other methods.

The presence of magnetite and ilmenite-hematite intergrowths in the surnamite-bearing pegmatite, e.g., 2292C, suggest that it could have been relatively oxidized during the granulite-facies metamorphism (Grew et al. 2000). Moreover, the nearly identical $Fe^{3+}/\Sigma Fe$ ratios of surinamite in samples 12207 and 2292C suggest that oxygen fugacity varied little from one part of the pegmatite to another. However, differences in the Fe_2O_3 contents of sillimanite from one part of the pegmatite to another, or even within a given section, appear to argue

TABLE 1. Compositions of studied surinamite

Sample	12207								2292C
Grain–analysis	1–1	1–2	2–1	2–2	3–1	3–2	Avg.	St. dev.	
No. points	10	10	10	10	10	10			5
					wt%				
SiO_2	32.98	32.26	32.52	32.25	32.80	32.94	32.63	0.33	31.32
P_2O_5	0.15	0.15	0.18	0.18	0.26	0.26	0.20	0.05	0.33
TiO_2	0.00	0.00	0.00	0.00	0.00	0.00	0.00	0.00	0.00
Al_2O_3	34.41	34.60	34.49	34.96	34.64	34.74	34.64	0.19	32.82
Fe_2O_3 (calc)	3.23	4.08	3.26	3.86	2.65	2.14	3.20		5.59
FeO (calc)	6.55	5.95	6.35	5.85	7.21	7.83	6.63		9.14
MnO	0.17	0.18	0.19	0.20	0.17	0.15	0.18	0.02	0.17
MgO	18.48	18.31	18.30	18.39	18.10	17.86	18.24	0.23	16.08
CaO	0.06	0.09	0.07	0.07	0.07	0.09	0.08	0.01	0.08
BeO (calc)	4.55	4.53	4.52	4.54	4.54	4.54	4.54		4.44
Sum	100.59	100.14	99.89	100.30	100.46	100.55	100.32		99.97
FeO (meas)	9.46	9.61	9.29	9.32	9.60	9.76	9.51	0.18	14.17
				Formula proportions based on a 11 cations and 16 oxygen atoms					
Si	3.017	2.967	2.995	2.957	3.006	3.019	2.994		2.944
P	0.012	0.012	0.014	0.014	0.020	0.020	0.015		0.027
Ti	0.000	0.000	0.000	0.000	0.000	0.000	0.000		0.000
Al	3.709	3.750	3.743	3.778	3.743	3.753	3.746		3.636
Fe^{3+}	0.222	0.282	0.226	0.266	0.183	0.148	0.221		0.395
Fe^{2+}	0.501	0.457	0.489	0.448	0.553	0.600	0.508		0.719
Mn	0.014	0.014	0.015	0.016	0.013	0.012	0.014		0.014
Mg	2.520	2.510	2.511	2.513	2.474	2.440	2.495		2.254
Ca	0.006	0.008	0.007	0.007	0.007	0.009	0.007		0.008
Be	1.000	1.000	1.000	1.000	1.000	1.000	1.000		1.002
Sum	11.000	11.000	11.000	11.000	11.000	11.000	11.000		11.000
$Fe^{3+}/\Sigma Fe$ (stoich)	0.31	0.38	0.32	0.37	0.25	0.20	0.30	0.06	0.35
$Fe^{3+}/\Sigma Fe$ (other)							0.31		0.35
$Mg/(Mg + Fe^{2+})$	0.834	0.846	0.837	0.849	0.817	0.803	0.831		0.758

Note: Fe^{3+}/Fe^{2+} ratio and Be content were calculated from stoichiometry (see text), except for sample 2292C, in which Be was determined from refinement of the crystal structure. $Fe^{3+}/\Sigma Fe$ (other) ratios were determined by room-temperature Mössbauer spectroscopy (12207) and refinement of the crystal structure (2292C). Each of three grains was analyzed twice for all constituents except P, which was analyzed once. Grain 2292C was used in the crystal structure refinement. The analysis for 2292C is from Grew et al. (2000).

against uniformity in oxygen fugacity. For example, the Fe_2O_3 content of five sillimanite grains near the three analyzed surinamite grains in 12207 ranges from 0.76 to 1.54 wt%. A possible explanation for the apparent discrepancy is that total Fe content varied from one part of the pegmatite to another, even on the scale of a thin section. Thus, surinamite total Fe content varied, but its $Fe^{3+}/\Sigma Fe$ ratio would remain relatively constant if oxygen fugacity were uniform throughout. In Fe-rich parts of the pegmatite, the capacity of surinamite to incorporate Fe^{2+} and Fe^{3+} was exceeded and the "extra" Fe formed magnetite and hematite, e.g., 2292C, whereas 12207 is an example in which this saturation was not reached and Fe oxides are absent. The assemblage quartz + garnet + surinamite + sillimanite has a high-variance in the subsystem MgO-FeO-Fe_2O_3-Al_2O_3-BeO-SiO_2, and contents of Fe^{2+} and Fe^{3+} in a given mineral depends on availability of Fe^{2+} and Fe^{3+} in the immediate environment, e.g., Fe^{3+} for sillimanite, even though $Fe^{3+}/\Sigma Fe$ ratio in a mineral containing Fe in both valence states depends only on oxygen fugacity. In summary, minerals containing variable amounts of both Fe^{2+} and Fe^{3+}, e.g., surinamite in the Antarctic pegmatite, would be a better monitor of oxygen fugacity than minerals that contain only Fe^{2+} or only Fe^{3+}.

CRYSTALLOGRAPHY

Powder X-ray diffraction

A few grains of surinamite were extracted from sample 2292C (Grew 1981) and an X-ray powder pattern was recorded with a Guinier-Hägg camera using Cu$K\alpha_1$ radiation and Si as an internal standard. Fluorescence due to the presence of Fe and the large fraction of very weak diffraction lines in the powder pattern limited the number of observable lines to 20 in the angular range $30 < 2\theta < 60°$. Nevertheless, the refined unit-cell parameters (Table 2) are in good agreement with those previously determined by Moore and Araki (1983) for a crystal from the same sample [$a = 9.916(1)$, $b = 11.384(1)$, $c = 9.631(1)$ Å, $\beta = 109.30(1)°$]. The indexing of the powder pattern was later confirmed by comparison to a calculated pattern based on the refined crystal structure.

Structure refinement by single crystal X-ray diffraction

A small, irregular blue-green crystal of surinamite (140 × 90 × 20 μm) was selected from sample 2292C (Grew 1981) and mounted on a Siemens diffractometer equipped with a Mo$K\alpha$ rotating anode and a SMART area detector. To obtain good intensity measurements of the numerous weak reflections, the X-ray generator was run at 15 kW and the exposure time for individual frames of the area detector was set at 60 s. Details of the data collection are summarized in Table 2.

After correcting the raw intensity data for absorption with the SADABS program (Sheldrick 1996), the structure refinement was carried out with the SHELXL93 software (Sheldrick 1993) using the atomic positions previously refined by Moore and Araki (1983) as a starting model. The present refinement was done on the basis of a simplified chemical composition, viz., $Mg_{2.26}Fe_{1.13}Al_{3.61}Be_{1.00}Si_{3.00}O_{16}$, in which the small amounts

TABLE 2. Single-crystal X-ray data and structure refinement of surinamite

Chemical formula	$Mg_{2.26}Fe_{1.13}Al_{3.61}Be_{1.00}Si_{3.00}O_{16}$*
Space group	*P*2/*n*
a (Å)	9.915(2)
b (Å)	11.368(2)
c (Å)	9.617(2)
β (°)	109.30(2)
V (Å^3)	1023.1
Z	4
Calculated density (g/cm^3)	3.67
m (mm^{-1}) (Mo*K*α)	2.58
2θ max (°)	72.80
h_{min}, h_{max}	–16, 15
k_{min}, k_{max}	–18, 18
l_{min}, l_{max}	–12, 15
Observed reflections	22537
Independent reflections	4882
Absorption correction	based on equivalent reflections (SADABS software)
T_{min}, T_{max}	0.5025, 0.8682
R_{int}	0.039
Parameters refined	261 in final anisotropic cycles
Reflections used	4876
Reflections with $F_o > 4\sigma(F_o)$	4073
Weighting scheme	$[\sigma^2(F_o^2) + (0.037\ P)^2 + 0.39\ P]^{-1}$ with $P = [\max(F_o^2,0) + 2F_c^2]/3$
$R(F)$ [$F_o > 4\sigma(F_o)$]	0.030
$wR(F^2)$ (all)	0.074
$(\Delta\rho)_{min}$ (e.Å^{-3})	–0.86
$(\Delta\rho)_{max}$ (e.Å^{-3})	0.68

* Simplified chemical formula based on 11 cations. The small amounts of Ca, Mn and P in the analytical data (sample 2292C in Table 1) have been ignored. The simplified formula implies 0.74 Fe^{2+} + 0.39 Fe^{3+}, in good agreement with the analytical formula.

TABLE 3. Site occupancies*, average bond lengths (Å), and polyhedral distortions† in surinamite

	%Be	%Al	%Si	<T-O>	<λ>	σ^2
T1	97	–	3	1.642	1.001	3.13
T2	–	–	100	1.632	1.003	13.32
T3	–	3	97	1.645	1.001	2.65
T4	–	–	100	1.634	1.003	10.71
T5	3	97	–	1.754	1.005	18.31
	%Mg	%Fe	%Al	<M-O>	<λ>	σ^2
M1	57	43	–	2.186	1.037	115.86
M2	–	23	77	1.952	1.018	54.51
M3	–	12	88	1.935	1.007	22.65
M4	91	9	–	2.056	1.016	49.30
M5	89	11	–	2.107	1.025	84.33
M6	–	3	97	1.912	1.012	38.82
M7	72	28	–	2.101	1.028	85.31
M8	88	12	–	2.085	1.018	65.27
M9	–	6	94	1.926	1.010	32.44

* The site labeling follows that of Moore and Araki (1983).
† As defined by Robinson et al. (1971): <λ> = mean quadratic elongation and σ^2 = angular variance (in degrees).

of Mn and Ca determined in the electron microprobe analysis (Table 1) were included with Fe and Mg, respectively. The slightly larger Si/Al ratio relative to the analytical formula results from replacing the small amount of P (cf., Table 1) by the minor tetrahedral substitution P + Al = 2Si. The twenty-four octahedral cations (distributed over nine M sites) plus the twenty tetrahedral cations (distributed over five T sites) and the sixty-four oxygen atoms of the surinamite unit cell lead to a coordination formula of $^{VI}(Mg_{2.26}Fe_{1.13}Al_{2.61})O^{IV}(Al_{1.00}Be_{1.00}Si_{3.00})O_{15}$, with $Z = 4$. The assumed stoichiometry of 11 cations for 16 O atoms (i.e., with all sites fully occupied) requires that Fe be present as 0.74 Fe^{2+} + 0.39 Fe^{3+}, which is in good agreement with the refined site occupancies and the Mössbauer spectroscopy data (see below).

The occupancies of the individual cation sites were refined on the basis of the coordination formula given above, with the additional constraint of equal U_{eq} parameters for all M sites on one hand, and all T sites on the other. The refinement of the tetrahedral Be occupancies quickly converged to 97% Be on T1, 3% Be on T5 and 0% Be on the remaining sites, with e.s.d. values better than 0.5%. The average <T-O> distances indicated that T5 was Al rich (<T5-O> = 1.75 Å) and that T2 and T4 contained only Si (<T-O> = 1.63 Å). A minor Al/Si mixing on T3 was determined from the compositional constraint of the overall tetrahedral content, and by refining the U_{eq} parameters of the individual T sites. The final T-site occupancies and the <T-O> distances are listed in Table 3.

The refinement of the octahedral Fe occupancies was initially done against a random Mg/Al distribution on the M1-9 sites. A full occupancy was assumed for all sites but no constraint was imposed on the total Fe content. The Fe occupancies converged smoothly with final e.s.d. values less than 0.2%, and the resulting total Fe content of 1.127 Fe for 16 oxygen atoms agreed very well with the overall chemical composition. At that stage, inspection of the average <M-O> distances revealed the presence of two groups of octahedral sites: M1, M4, M5, M7, and M8 with longer <M-O> distances of 2.05–2.18 Å, which were assigned to Mg + Fe^{2+} occupancies; and M2, M3, M6, and M9 with shorter <M-O> distances of 1.91–1.95 Å, which were assigned to Al + Fe^{3+} occupancies. This particular cation distribution yields a total octahedral content of $Mg_{2.27}Fe^{2+}_{0.73}Fe^{3+}_{0.40}Al_{2.60}$ for 16 oxygen atoms, in excellent agreement with the overall chemical composition. Although some very minor Mg/Al or Fe^{2+}/Fe^{3+} mixing may well occur on the octahedral sites, no attempt has been made to determine this mixing further. The final M-site occupancies and the <M-O> distances are listed in Table 3.

In the final refinement cycles, all cation site occupancies were fixed at their refined values, and a fully anisotropic refinement was carried out for all cation and oxygen sites. The final reliability indices are given in Table 2. The corresponding atom coordinates and U_{eq} parameters are listed in Table 4, the anisotropic U_{ij} parameters are in Table 5.

The present refinement of the surinamite structure agrees very well with the previous study by Moore and Araki (1983) in terms of the atomic coordinates of the cation and oxygen sites. The two refinements, however, differ significantly in several other aspects. First, Moore and Araki had assumed that all Fe was present as Fe^{2+}, which nevertheless resulted in a slight excess of positive charges in the unit cell (128.9 for 64 O atoms). In contrast, the present X-ray site populations imply the presence of substantial Fe^{3+}, which is supported by Mössbauer spectroscopy. Second, Moore and Araki had tentatively concluded that few tetrahedral vacancies were present on the Al-rich T5 site in spite of a significantly smaller B_{eq} parameter for that site. No evidence for such vacancies was found in the present work and, instead, Be has been identified as a minor substituent on the T5 site. The tetrahedral occupancies refined

in this work correlate well with the <T-O> distances and yield more uniform values of the U_{eq} parameters for all five T sites. Finally, the octahedral site occupancies refined in this study are in general agreement with those determined by Moore and Araki, with the exception of the M4 site. Whereas the population of that site had been assigned as 100% Al by Moore and Araki, the present refinement yields a population of 91% Mg + 9% Fe^{2+}, in better agreement with the <M4-O> distance of 2.06 Å (Table 3). Overall, the U_{eq} parameters for all nine octahedral sites are also more uniform in the present refinement and all the octahedral occupancies correlate well with the <M-O> distances.

TABLE 4. Atomic coordinates and isotropic displacement parameters (in Å^2) for surinamite

Site*	*x*	*y*	*z*	U_{eq}
M1	0.47690(3)	0.65771(3)	0.25890(3)	0.00689(6)
M2	0.50136(3)	0.37756(3)	0.26862(3)	0.00608(6)
M3	0.50233(4)	0.11433(3)	0.25462(3)	0.00605(7)
M4	0.2500	0.25304(5)	0.2500	0.00642(10)
M5	0.2500	0.96605(5)	0.2500	0.00647(10)
M6	0.7500	0.51185(5)	0.2500	0.00607(9)
M7	0.7500	0.25557(4)	0.2500	0.00648(8)
M8	0.7500	0.97415(5)	0.2500	0.00634(9)
M9	0.0000	0.5000	0.5000	0.00601(9)
T1	0.3237(2)	0.75235(13)	0.45699(15)	0.0050(2)
T2	0.07701(4)	0.88375(3)	0.44837(3)	0.00462(7)
T3	0.30667(4)	0.50194(3)	0.43710(3)	0.00495(7)
T4	0.56921(4)	0.87998(3)	0.44768(3)	0.00461(7)
T5	0.83025(4)	0.74469(4)	0.45266(4)	0.00445(7)
O1	0.11660(10)	0.99888(9)	0.37094(9)	0.0064(2)
O2	0.61422(10)	0.99433(9)	0.37211(9)	0.0063(2)
O3	0.87653(10)	0.11306(8)	0.37006(9)	0.0060(2)
O4	0.37590(10)	0.11535(8)	0.37102(9)	0.0060(2)
O5	0.90338(10)	0.86363(8)	0.38764(10)	0.0064(2)
O6	0.39921(10)	0.85516(9)	0.38787(10)	0.0067(2)
O7	0.61033(10)	0.24682(9)	0.36261(10)	0.0066(2)
O8	0.64468(10)	0.76550(8)	0.39776(10)	0.0068(2)
O9	0.10797(10)	0.25107(8)	0.35475(10)	0.0062(2)
O10	0.14979(10)	0.76909(9)	0.40325(10)	0.0070(2)
O11	0.35862(10)	0.62618(8)	0.39168(10)	0.0070(2)
O12	0.37004(10)	0.39300(9)	0.36835(10)	0.0074(2)
O13	0.88128(10)	0.61979(8)	0.37268(10)	0.0062(2)
O14	0.88404(10)	0.40002(8)	0.35400(9)	0.0060(2)
O15	0.63220(10)	0.50604(9)	0.37974(9)	0.0072(2)
O16	0.12766(10)	0.49863(9)	0.38238(9)	0.0068(2)

* The site labeling follows that of Moore and Araki (1983).

Description of the surinamite structure

Part of the surinamite structure is illustrated in Figure 2. Individual octahedral and tetrahedral bond distances and selected bond angles are listed in Table 6. The main features of the structure have been described in detail previously (Moore and Araki 1983): the structure is based on an oxygen cubic close-packing with [100] branched tetrahedral chains separated by octahedral walls. Alternatively, the structure can be viewed as a regular intergrowth of spinel-like and pyroxene-like (010) lamellae, which emphasizes the polysomatic relationship with the sapphirine structure (Christy and Putnis 1988; Barbier 1996, 1998).

The polyhedral distortions in the surinamite structure are of interest in connection with the interpretation of the optical absorption spectra and the Mössbauer spectra (see below). These distortions can be described by calculating the mean quadratic elongation and the bond-angle variance (Robinson et al. 1971) of the individual octahedra and tetrahedra. The results clearly show that the five tetrahedral sites are fairly regular, whereas the nine octahedral sites display a wide range of distortions (Table 3). Overall, the larger Fe^{2+}-bearing sites (M1, M4, M5, M7, M8) are more distorted from ideal octahedral geometry than the smaller Fe^{3+}-bearing sites (M2, M3, M6, M9), both in terms of bond distances and bond angles. In both groups, the degree of distortion generally correlates with the Fe content.

OPTICAL SPECTROSCOPY

Polarized optical absorption spectra of surinamite sample 12207 from Christmas Point were obtained at room tempera-

TABLE 5. Anisotropic displacement parameters for surinamite

	U_{11}	U_{22}	U_{33}	U_{23}	U_{13}	U_{12}
M1	0.00647(12)	0.00902(13)	0.00517(10)	0.00020(9)	0.00189(9)	–0.00087(9)
M2	0.00525(14)	0.00683(14)	0.00629(12)	–0.00018(10)	0.00209(10)	–0.00034(10)
M3	0.0055(2)	0.0071(2)	0.00549(13)	0.00019(11)	0.00173(12)	0.00005(11)
M4	0.0054(2)	0.0078(2)	0.0065(2)	0.000	0.0027(2)	0.000
M5	0.0050(2)	0.0086(2)	0.0057(2)	0.000	0.0016(2)	0.000
M6	0.0051(2)	0.0072(2)	0.0051(2)	0.000	0.0006(2)	0.000
M7	0.0053(2)	0.0067(2)	0.0081(2)	0.000	0.0031(2)	0.000
M8	0.0050(2)	0.0079(2)	0.0059(2)	0.000	0.0016(2)	0.000
M9	0.0057(2)	0.0074(2)	0.0042(2)	–0.0004(2)	0.0007(2)	0.0001(2)
T1	0.0034(6)	0.0064(6)	0.0044(5)	0.0007(4)	0.0005(4)	0.0002(4)
T2	0.00431(14)	0.00617(15)	0.00316(12)	0.00009(10)	0.00093(11)	–0.00002(10)
T3	0.00460(14)	0.00664(15)	0.00332(12)	–0.00018(11)	0.00092(11)	–0.00015(11)
T4	0.00435(14)	0.00618(15)	0.00304(12)	0.00007(10)	0.00087(11)	0.00024(11)
T5	0.0045(2)	0.0053(2)	0.00331(14)	–0.00005(12)	0.00105(13)	0.00020(12)
O1	0.0058(4)	0.0078(4)	0.0058(3)	0.0008(3)	0.0023(3)	–0.0001(3)
O2	0.0061(4)	0.0071(4)	0.0060(3)	–0.0012(3)	0.0024(3)	0.0000(3)
O3	0.0056(4)	0.0082(4)	0.0038(3)	–0.0004(3)	0.0010(3)	–0.0002(3)
O4	0.0057(4)	0.0083(4)	0.0039(3)	0.0000(3)	0.0012(3)	0.0002(3)
O5	0.0055(4)	0.0074(4)	0.0059(3)	0.0013(3)	0.0013(3)	0.0001(3)
O6	0.0047(4)	0.0089(4)	0.0058(3)	–0.0011(3)	0.0006(3)	0.0006(3)
O7	0.0056(4)	0.0096(4)	0.0045(3)	0.0000(3)	0.0013(3)	0.0007(3)
O8	0.0059(4)	0.0081(4)	0.0071(3)	0.0000(3)	0.0029(3)	0.0003(3)
O12	0.0067(4)	0.0085(4)	0.0062(3)	0.0008(3)	0.0011(3)	–0.0002(3)
O13	0.0058(4)	0.0067(4)	0.0055(3)	–0.0005(3)	0.0010(3)	0.0003(3)
O14	0.0060(4)	0.0069(4)	0.0049(3)	0.0003(3)	0.0013(3)	0.0002(3)
O15	0.0069(4)	0.0106(4)	0.0040(3)	0.0002(3)	0.0018(3)	0.0003(3)
O16	0.0056(4)	0.0092(4)	0.0056(3)	–0.0005(3)	0.0020(3)	–0.0006(3)

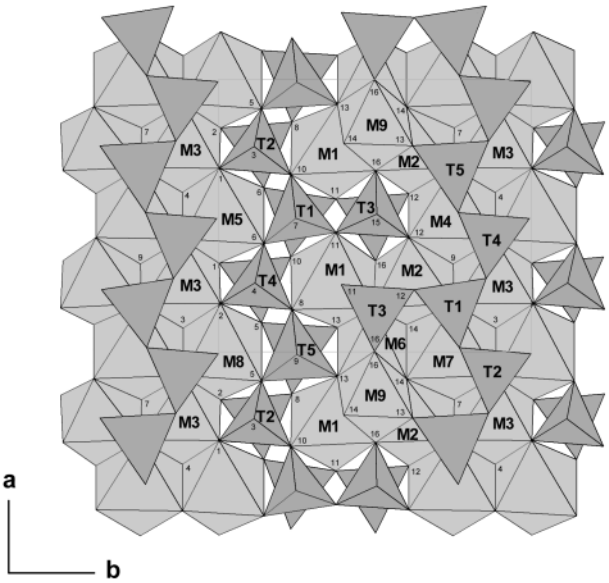

FIGURE 2. Part of the surinamite structure viewed along the [103] direction, nearly perpendicular to the (*a*-*b*) plane. Small number at the corners of the polyhedra refer to the oxygen positions.

TABLE 6. Bond lengths (Å) and tetrahedral chain bond angles (°) in surinamite

M1-O11	2.031(1)	M8-O2	2.071(1)
M1-O10	2.078(1)	M8-O2	2.071(1)
M1-O8	2.141(1)	M8-O5	2.077(1)
M1-O13	2.223(1)	M8-O5	2.077(1)
M1-O16	2.294(1)	M8-O3	2.108(1)
M1-O15	2.348(1)	M8-O3	2.108(1)
M2-O12	1.863(1)	M9-O14	1.876(1)
M2-O7	1.883(1)	M9-O14	1.876(1)
M2-O14	1.906(1)	M9-O13	1.946(1)
M2-O9	1.949(1)	M9-O13	1.946(1)
M2-O15	2.010(1)	M9-O16	1.957(1)
M2-O16	2.100(1)	M9-O16	1.957(1)
M3-O2	1.881(1)	T1-O10	1.639(2)
M3-O1	1.905(1)	T1-O7	1.639(2)
M3-O4	1.937(1)	T1-O6	1.642(2)
M3-O7	1.939(1)	T1-O11	1.648(2)
M3-O3	1.958(1)		
M3-O9	1.989(1)	T2-O1	1.617(1)
		T2-O10	1.617(1)
M4-O9	1.984(1)	T2-O5	1.641(1)
M4-O9	1.984(1)	T2-O3	1.653(1)
M4-O12	2.085(1)		
M4-O12	2.085(1)	T3-O11	1.612(1)
M4-O4	2.098(1)	T3-O12	1.625(1)
M4-O4	2.098(1)	T3-O15	1.665(1)
		T3-O16	1.677(1)
M5-O6	2.059(1)		
M5-O6	2.059(1)	T4-O6	1.616(1)
M5-O1	2.064(1)	T4-O2	1.622(1)
M5-O1	2.064(1)	T4-O4	1.647(1)
M5-O4	2.198(1)	T4-O8	1.650(1)
M5-O4	2.198(1)		
		T5-O5	1.745(1)
M6-O14	1.872(1)	T5-O9	1.749(1)
M6-O14	1.872(1)	T5-O8	1.754(1)
M6-O13	1.891(1)	T5-O13	1.767(1)
M6-O13	1.891(1)		
M6-O15	1.972(1)	T2-O5-T5 119.5(1)	
M6-O15	1.972(1)	T1-O6-T4 122.8(1)	
		T4-O8-T5 123.4(1)	
M7-O7	2.023(1)	T1-O10-T2 121.7(1)	
M7-O7	2.023(1)		
M7-O3	2.139(1)		
M7-O3	2.139(1)		
M7-O14	2.141(1)		
M7-O14	2.141(1)		

ture directly from a polished petrographic thin-section of 30 μm thickness (Fig. 1), as determined by means of a digital micrometer. Optical orientations of the two measured single crystal grains were determined by applying interference figures obtained in conoscopic illumination. All spectra were recorded with a Zeiss MPM800 single-beam spectrometer using Zeiss Ultrafluar 10× lenses as objective and condenser and a Glan-Thompson prism as polarizer. In the UV/VIS-spectral range, a 75W Xenon arc lamp served as a light source and a photomultiplier as detector. In the NIR spectral region (12 500–5000 cm^{-1}), a 100W halogen lamp was used as a light source and light detection was achieved by means of a photoconductive PbS cell. Spectra were recorded at a spectral resolution of 2.5 nm in the UV/VIS range and 5 nm in the NIR region. The measured spot was kept constant at 40 μm.

Recorded spectra were fitted using the peak resolution program Jandel PeakFit 4.0. In the fitting process, all bands were assumed to be of Gaussian shape. The recorded UV-absorption edges were also fitted with Gaussian functions.

The resultant absorption spectra show a very strong anisotropy (Fig. 3). Five prominent features are recorded in the low energy range (below 18 000 cm^{-1}) of the spectra (Fig. 4). Two of these bands, at 17 900 and 13 500 cm^{-1}, are quite broad (see Table 7). The one at higher energy is strongly polarized in E||Y, whereas the other is polarized Z > Y. The absorption bands at 6700, 8500, and 10 500 cm^{-1} are less strongly polarized with Z > Y > X and are characterized by smaller half bandwidths (Table 7). The bandwidths, energies, intensities, and anisotropic behavior are all strong indications that the bands at 17 900 and 13 500 cm^{-1} are caused by IVCT processes (Burns 1993). Furthermore, the low to negligible contents of other transition elements in the analyzed surinamite sample restricts the possible IVCT processes responsible for these bands to electron transfers in Fe^{2+}-Fe^{3+} clusters.

The present crystal structure refinement of surinamite shows that there exists many different M(Fe^{2+})-M(Fe^{3+}) clusters. Several of these M-M pairs are found at low concentrations and are unlikely to contribute significantly to the absorption. With the exception of the M1-M9-cluster (M-M vector in the *b*-*c* plane), they all have M-M vectors within the crystallographic *a*-*b* plane (Fig. 2). In terms of M-M distances and vector directions, these clusters can be divided into two types (Table 8). One type of clusters (M1-M2 and M7-M6) display M-M vectors coinciding or being very close to the crystallographic b-axis, which in turn coincides with the optical Y-direction (de Roever et al. 1976). The other type comprises clusters for which the M-M vectors are at an angle of ~60° to the b (or Y)-direction. Based on the fact that absorption bands caused by IVCT processes are strongly polarized along the M-M vectors, absorption bands due to the first type of clusters are predicted to

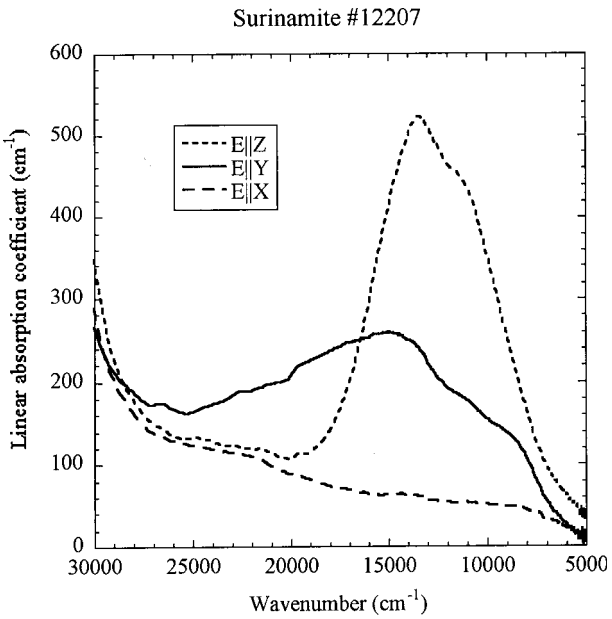

FIGURE 3. Polarized optical absorption spectra of surinamite 12207.

be observed in only E||Y-spectra. IVCT bands caused by electron transfers in the second type of clusters are expected to show the polarization Z > Y, with an intensity ratio (I_Z:I_Y) of approximately 3:1. The broad absorption bands observed in our surinamite spectra display intensity distributions in very good agreement with these predictions. The band at 17 900 cm^{-1}, which is only observed for E||Y, is accordingly assigned to a Fe^{2+}(M1)-Fe^{3+}(M2) IVCT process. Compared to the M1-M2 pair concentration, the concentration of the additional cluster showing a similar M-M vector orientation, M7-M6, is extremely low and it is likely to contribute very weakly to the spectrum. The absorption band at ~13 500 cm^{-1}, which displays an I_Z:I_Y-ratio of ~2.5 is consequently assigned to IVCT processes in the second type of clusters. Based on the cation occupancies retrieved from the structure refinement, IVCT processes in two (M7-M2 and M7-M3) of these seven different M-M clusters are expected to provide most of the band intensity observed at this wavenumber.

There are several possible explanations for the large energy difference between the two proposed IVCT bands. Although Fe^{2+} and Fe^{3+} are located in edge-sharing distorted octahedral sites and the ligands involved are of similar character, the M1-M2 distances (3.19 Å) are considerably longer than M7-M2 and M7-M3 distances (2.89 and 2.95 Å). It has been suggested that Fe^{2+}-Fe^{3+} IVCT energies depend on donor-acceptor distances (e.g., Smith and Strens 1976). However, later spectroscopic studies on many Fe- and Ti-bearing minerals (Mattson and Rossman 1987a) indicate that donor-acceptor distances have little influence on the IVCT energy, but rather relate to the type of mutual M-M contacts. An alternative explanation for the presence of Fe^{2+}-Fe^{3+} IVCT bands at two distinct energy regions is anisotropic polymerization of octahedral sites containing Fe^{2+} or Fe^{3+} in the surinamite structure. Along the b-

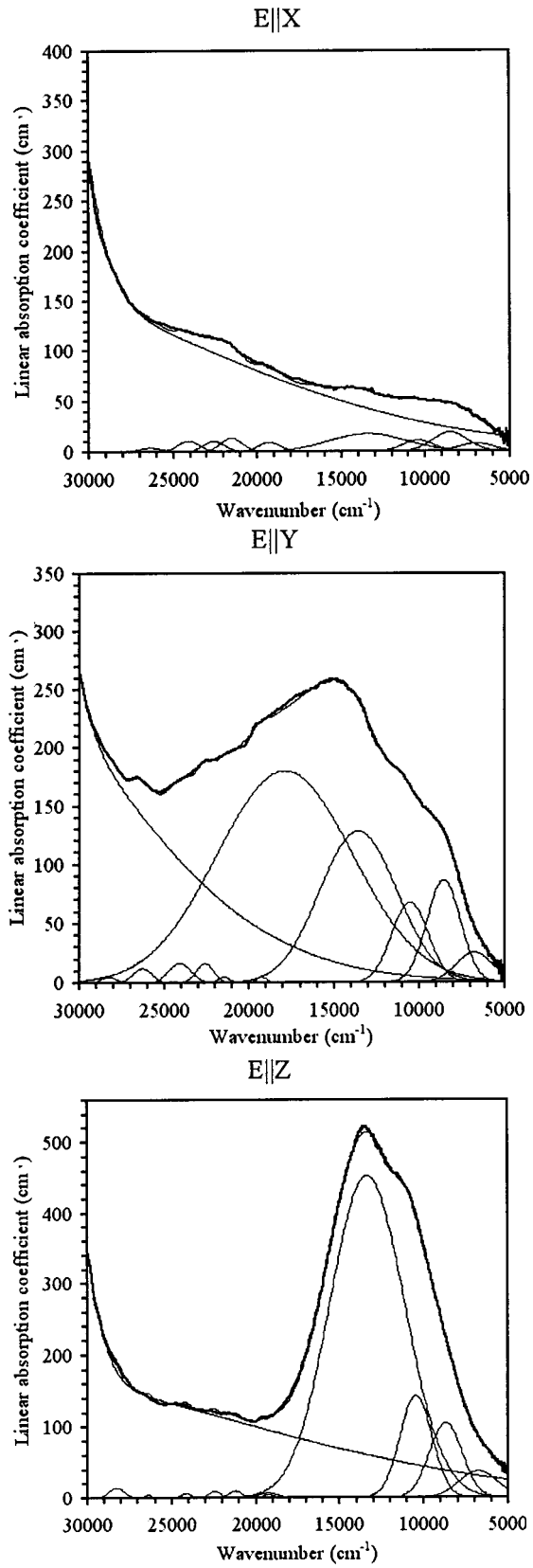

FIGURE 4. Fitted optical absorption spectra, E||X (**top**), Y (**middle**), and Z (**bottom**), of surinamite 12207.

TABLE 7. Characteristics of Fe^{2+}-Fe^{3+} IVCT and spin-allowed Fe^{2+} *d-d* bands in surinamite

Polarization	position (ν) (cm^{-1})	Band width ($\omega_{1/2}$) (cm^{-1})	Net linear absorption coeff (α_{net}) (cm^{-1})
E‖X	6980	2360	8
	8550	2430	19
	10450	2160	11
	13450	5410	18
E‖Y	6790	2450	25
	8560	2290	87
	10530	2490	68
	13580	5330	128
	17920	9350	180
E‖Z	6790	2670	37
	8710	2250	105
	10470	2220	143
	13350	5210	453

TABLE 8. Metal-metal distances, vector orientations and pair concentrations of Fe^{2+}-Fe^{3+} clusters in surinamite

Fe^{2+}-Fe^{3+} cluster	M-M distance (Å)	M-M vector∠b (°)	$[Fe^{2+}][Fe^{3+}]$ ($apfu^2$)
M1-M2	3.192	3.1	1.58
M1-M6	3.201	58.8	0.10
M4-M2	2.821	59.4	0.17
M4-M3	2.945	57.6	0.09
M5-M3	3.004	55.9	0.11
M7-M2	2.885	61.0	0.51
M7-M3	2.947	57.0	0.27
M7-M6	2.912	0.0	0.03
M8-M3	2.940	57.2	0.12

direction (= optical Y-direction), Fe^{2+}-Fe^{3+} clusters are restricted to the pair constellations Fe^{2+}(M1)-Fe^{3+}(M2) and Fe^{2+}(M7)-Fe^{3+}(M6), while longer sequences of alternating Fe^{2+} and Fe^{3+}-centered sites may occur within the octahedral walls along the crystallographic a axis, e.g., Fe^{2+}(M7)-Fe^{3+}(M2)-Fe^{2+}(M7)-Fe^{3+}(M2). The observed IVCT band at lower energy could result from charge-transfer processes between cations in trimers or larger clusters rather than in M-M pairs. Such IVCT transitions are likely to occur at lower energies than corresponding ones in discrete M-M pairs (Amthauer and Rossman 1984).

The three less-polarized absorption bands recorded at 6800, 8500, and 10 500 cm^{-1} are characterized by energies, band widths, and intensities characteristic of spin-allowed *d-d* electron transitions in octahedrally coordinated Fe^{2+} in many silicate minerals (Burns 1993). The bandwidths of the three bands (Table 7) are slightly anomalous, approximately 50% higher than expected, which may be attributed to the fact that Fe^{2+} is distributed over several octahedral sites in surinamite. In addition, the linear absorption coefficients recorded for these bands in E‖Y and E‖Z spectra (Table 7) are enhanced, which may be ascribed to electronic exchange coupling with neighboring Fe^{3+}cations that has been observed for the spin-allowed *d-d* transitions in Fe^{2+} in tourmaline (Mattson and Rossman 1987b).

Our structural refinement of surinamite shows that the Fe^{2+}-bearing M sites differ in terms of degree of distortion from O_h-symmetry as well as in mean M-O distance (Table 3). This will cause energy variations for Fe^{2+} *d-d* transitions at various sites. The Fe^{2+}-absorption bands recorded in the present spectra are consequently considered as composite bands, to which several strongly overlapping *d-d* bands contribute. These closely spaced bands are each related to specific electronic transitions to the split electronic E_g-levels in Fe^{2+} at the M1, M4, M5, M7, and M8 sites. On the basis of site occupancies, as obtained from our structural refinement and Mössbauer spectra, it is proposed that Fe^{2+} at the M1-site, which constitutes approximately 60% of the Fe^{2+} content in the sample, will give the strongest contribution to the NIR-spectrum.

In addition to the five strong bands discussed above, several closely spaced and relatively narrow bands of relatively low intensity are observed in the surinamite spectra at higher energies, above 19 000 cm^{-1} (Figs. 3 and 4). These bands, occurring at approximately 19 300, 21 300, 22 600, 24 200, 26 400, and 28 300 cm^{-1} most likely mark spin-forbidden *d-d* transitions in Fe^{2+} and/or Fe^{3+}.

From our optical absorption spectra some information regarding the orientation of the indicatrix axes with respect to the crystallographic axes in surinamite may be deduced. The present spectra have been obtained with the electric vector (E) of the incident polarized light parallel to each of the indicatrix axes (X, Y, and Z). As Y coincides with the crystallographic b axis, the optical directions X and Z must be located in a plane perpendicular to the crystallographic b axis (=Y). Our X spectrum shows very low intensities for bands that we assign to Fe^{2+}-Fe^{3+} charge transfer processes. In combination with the results of the structural refinement, this observation restricts the position of the optical X axis to being almost perpendicular to the crystallographic *a-b* plane (i.e., the plane of M-M vectors). Consequently, the angle between X and the crystallographic c axis is approximately 20°, which in turn restricts the Z axis to be at a very small angle to the crystallographic a axis. For the IVCT band at 13 500 cm^{-1}, we observe a slightly smaller Iz:Iy-ratio of 2.5 as compared to the expected (from structural considerations) value of 3.0 for Z = a. This observation indicates that the Z axis is at angle of ca. 5° to the crystallographic a axis.

Our optical absorption spectra demonstrate that the unusual color and pleochroism of surinamite is mainly due to absorption bands caused by intense Fe^{2+}-Fe^{3+} IVCT processes. In addition, surinamite spectra show unusually high transmission in the high-energy region of the visible spectral range (blue region). These combined properties result in transmission maxima in the region 400–500 nm, which cause the uncommon bluish-green and purplish color tones visible in Y and Z.

MÖSSBAUER SPECTROSCOPY

Mössbauer spectra were obtained at room temperature (ca. 295 K) and liquid nitrogen temperature (ca. 80 K) using a constant acceleration system working in conjunction with a 1024 Multi Channel Analyzer. A nominal 50 mCi ^{57}Co/Rh-source and a gas-filled proportional counter were used as source and detector in these experiments. The sample absorber consisted of a self-supporting pressed disc prepared of 7 mg surinamite powder and 160 mg acrylic transoptic powder (lucite), corresponding to an absorber thickness of approximately 0.5 mg Fe/cm^2. To minimize texture effects, which may be significant as a consequence of the perfect (010) cleavage in surinamite, the

spectra were recorded with the absorber at an angle of 54.7° to the incident gamma-rays (Ericsson and Wäppling 1976).

The surinamite powder used in the present absorber was obtained through crushing and sieving of a chip of sample 12207. A surinamite concentrate was obtained from the sieved fraction 100–150 μm using an isodynamic Frantz magnet. Subsequently, this concentrate was further refined by hand picking under a binocular microscope.

The raw data were folded and fitted using a computer program (Jernberg and Sundqvist 1983) assuming resonance absorption lines of Lorentzian shape and equal intensity and line width of the components of each quadrupole doublet. In addition, bandwidths of the quadrupole doublets were constrained to be equal. The velocity range of the sample spectra was calibrated against metallic iron (α-Fe) at room temperature.

The Mössbauer spectra recorded at room and liquid nitrogen temperature show a prominent high-velocity absorption and two slightly overlapping absorption regions at low velocities (Fig. 5). The shape of the high-velocity region indicates that it is composed of at least three partly overlapping absorption peaks. The almost resolved low-velocity absorption at approximately 1 mm/s is also characterized by an asymmetry, which indicates that at least two peaks contribute to this region. Overall, the spectral shapes suggest that at least five quadrupole doublets are required to obtain reasonable fits of the recorded spectra.

The complex nature of the surinamite crystal structure in combination with a distribution of Fe^{2+} and Fe^{3+} species over a considerable number of octahedral sites (Table 3) makes fitting of the Mössbauer spectra as well as assignments of fitted quadrupole doublets non-trivial. To derive a reasonable model for fitting and assignments of the spectra, we have performed several calculations that primarily use information from the structural refinement of surinamite as input data. From these data, combined with calculations of the d-orbital energies in Fe^{2+} at the Fe^{2+}-rich sites (M1, M4, M5, M7, and M8), further calculations of the local reduction factor, *F*, at room temperature for Fe^{2+} at these sites were performed according to the method of Ingalls (1964). The *F*-factor is considered as a good approximation for the Mössbauer quadrupole hyperfine parameter.

Our point-charge calculations (Shen et al. 1994) suggest that the splitting of the t_{2g}-orbitals in Fe^{2+} decreases in surinamite in the order M7~M4 > M1~M5 > M8. The calculated Δ_2/Δ_1-ratios vary between 3 and 6 except for Fe^{2+} at M8, which shows a high ratio of ~10 at a very small splitting (Δ_1-value) of the d_{xy} and d_{yz} orbitals. The results of our *F*-factor calculations (Ingalls 1964) for Fe^{2+} in surinamite indicate the following order of quadrupole splitting for absorption doublets caused by ferrous at the various Fe^{2+}-centered sites: M1~M5 > M4~M7 > M8. As a consequence of this scheme, quadrupole doublets due to Fe^{2+} at M1 and M5 and due to Fe^{2+} at M4 and M7 are predicted to be unresolved.

Assuming only Mg-Fe^{2+} and Al-Fe^{3+} mixing on octahedral sites (see above), our crystal-structure refinement of surinamite indicates that Fe^{3+} is present at four sites (M2, M3, M6, and M9) and is concentrated at M2 (cf., <M-O> bond distances in Table 3). The M2 site deviates more from octahedral symmetry than the other three, which have comparable site distortions. In contrast to the case for Fe^{2+}, the quadrupole splitting for Fe^{3+} is directly related to the local distortion parameter. Consequently, Fe^{3+} in surinamite is expected to give rise to two quadrupole doublets showing different quadrupole splitting parameters, with higher values for Fe^{3+} at the M2-site.

On the basis of our calculated *F*-factors for Fe^{2+} at various sites in surinamite and the structural information on the distor-

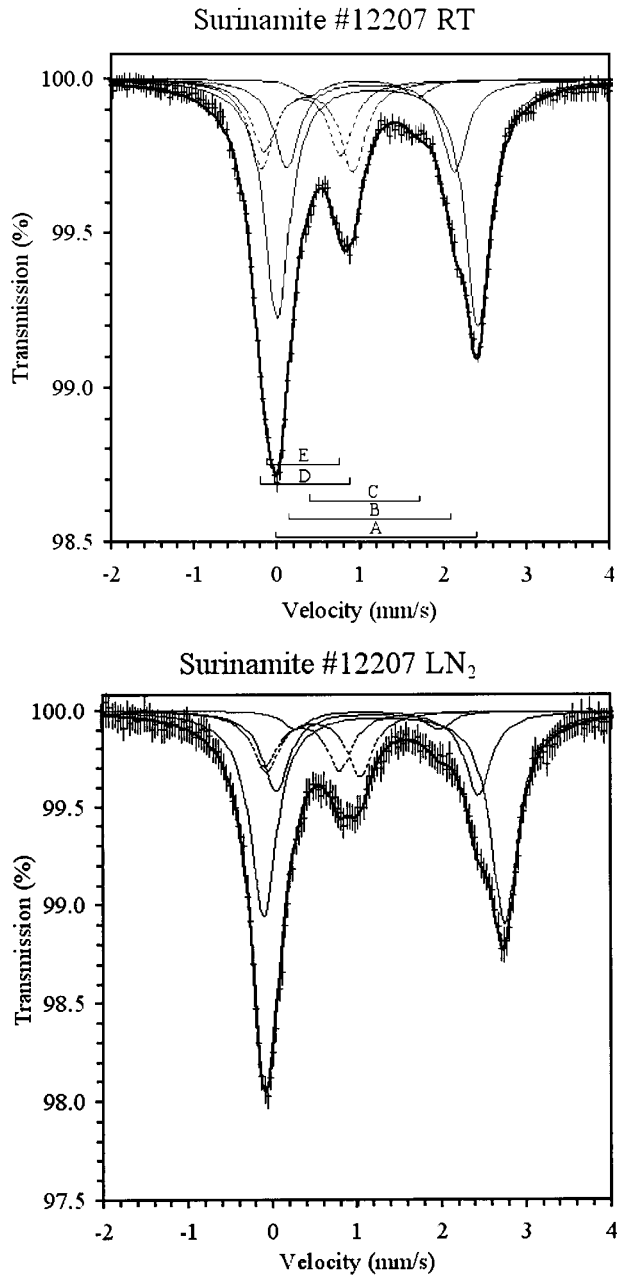

FIGURE 5. Fitted Mössbauer spectra of surinamite 12207 at room (**top**) and liquid nitrogen (**bottom**) temperatures. The crosses represent error bars for each data point. The bold solid line shows the sum of the fitted sub-spectra. The thin solid and broken lines represent fitted quadrupole doublets (sub-spectra) due to ferrous and ferric iron, respectively.

tion of Fe^{3+}-bearing sites, we have adopted a fitting model for the surinamite Mössbauer spectra that comprises three quadrupole doublets due to Fe^{2+} at the M1 + M5, M4 + M7, and M8 sites, as well as two absorption doublets due to Fe^{3+} at the M2 and M3 + M6 + M9 sites, respectively (Table 9). Fits of the surinamite spectra using this model converged at χ^2-values of 1.66 and 1.31 for the spectra recorded at room and liquid nitrogen temperature, respectively. Application of the present fitting model under the assumption of equal recoil-free fractions for Fe at the different sites results in an Fe distribution that is in very good agreement with data from our structural refinement. This assumption is reasonable in view of the comparable relative intensities of the different quadrupole sets in spectra recorded at the two different temperatures, which in turn suggests comparable Debye temperatures and, consequently, similar *F*-factors for Fe at different sites.

Most of the resulting values for the centroid shifts (CS) of the doublets A-C and D-E lie well within the range of values recorded for Fe^{2+} and Fe^{3+} at octahedral sites in many silicate minerals (e.g., Coey 1984), but a few approach the limits of these ranges. The room-temperature CS values of 0.31 and 0.36 mm/s assigned to Fe^{3+} at octahedral sites in surinamite are at the lower end of the range for octahedrally coordinated Fe^{3+} and approach values for Fe^{3+} at large tetrahedral sites (e.g., Tang Kai et al. 1980; Burns and Solberg 1990). A similar ambiguity pertains to the related mineral sapphirine. Our assignments in surinamite are consistent with the interpretation of Burns and Solberg (1990), who attributed the doublets having CS of 0.29–0.35 mm/s in two natural sapphirine samples to octahedrally coordinated Fe^{3+}. In contrast, Steffen et al. (1984) assigned doublets with CS of 0.27–0.30 mm/s in room-temperature spectra of synthetic sapphirine to Fe^{3+} at relatively large (mean T-O distances 1.72–1.76 Å) tetrahedral sites and argued that low centroid shifts for Fe^{3+} at octahedral sites should only be observed when the sites are very strongly distorted from O_h-symmetry. However, low CS for octahedral Fe^{3+} in silicates are not restricted to highly distorted sites, e.g., centroid shifts range from 0.31 to 0.36 mm/s for Fe^{3+} in skiagitic garnets (Woodland and O'Neill 1993). The extremely low quadrupole splitting of 0.18–0.25 mm/s for these doublets clearly shows that the octahedra in these garnets are very regular with negligible deviation from O_h-symmetry. Another example is Fe^{3+} at the octahedral M1A-site in chloritoid, for which the CS is 0.30 mm/s and the quadrupole splitting is 0.90 mm/s (Koch-Müller et al. 2000). The M1A-octahedron is similar in distortion and mean bond length (1.964 Å) to the smaller octahedral sites (M2, M3, M6, and M9) in surinamite. In summary, we conclude that the preponderance of available evidence is consistent with Fe^{3+} being located only at small octahedral sites in surinamite. If tetrahedral Fe^{3+} were present, the amounts are below the detection limits of Mössbauer spectroscopy (~0.03 apfu) and of crystal structure refinement (~3 at% for Fe vs. Al or Si) with the methods used in our study.

In addition, the room temperature CS of 1.20 mm/s for the quadrupole set A (Table 9) is high for octahedrally coordinated Fe^{2+}. However, quadrupole doublets displaying similar CS values have been assigned to octahedrally coordinated Fe^{2+} in several other silicates. For instance, CS values in the ranges 1.18–1.22 mm/s been recorded for quadrupole doublets due to octahedrally coordinated Fe^{2+} in room temperature Mössbauer spectra of babingtonite (Burns and Dyar 1991), cordierite (Goldman et al. 1977), and osumilite (Goldman and Rossman 1978). The results of Goldman et al. (1977) are confirmed by high CS values of ~1.34 mm/s in liquid nitrogen Mössbauer spectra of cordierite (Geiger et al. 2000). The octahedral sites in these minerals are characterized by relatively long mean M-O distances of 2.15–2.17 Å (Araki and Zoltai 1972; Armbruster and Oberhänsli 1988; cf., 2.186 Å for M1 in surinamite, Table 3).

The assignment of the C-doublet with a very low CS value of 1.03 mm/s in the room temperature spectrum (Table 9) is less obvious. Similar values have been recorded for quadrupole doublets due to Fe^{2+}at tetrahedral, pentahedral, and octahedral sites. The low intensity of this doublet in combination with the strong overlap of five bands in the low velocity range of the spectra results in a higher uncertainty for its parameters. In the absence of independent evidence for tetrahedrally coordinated Fe^{2+} in surinamite, and on the basis of the low quadrupole splitting, we tentatively assign doublet C to Fe^{2+} at the octahedral M8-site.

TABLE 9. Mössbauer parameters* and crystal structure Fe-ordering data for surinamite

	Fe^{2+} (A)	Fe^{2+} (B)	Fe^{2+} (C)	Fe^{3+} (D)	Fe^{3+} (E)
Room temperature (~295 K)					
I (%)	48	18	3	17	14
W (mm/s)	0.36	0.36	0.36	0.36	0.36
CS (mm/s)	1.20	1.12	1.03	0.36	0.31
Dq (mm/s)	2.42	2.02	1.30	1.09	0.92
Liquid nitrogen temperature (~80 K)					
I (%)	49	19	4	15	13
W (mm/s)	0.37	0.37	0.37	0.37	0.37
CS (mm/s)	1.32	1.24	1.12	0.47	0.39
Dq (mm/s)	2.86	2.41	1.71	1.12	0.90

Octahedral Fe contents (from Table 3)*

	Fe^{2+}	Fe^{2+}	Fe^{2+}	Fe^{3+}	Fe^{3+}
Sites	M1+M5	M4+M7	M8	M2	M3+M6+M9
Fraction of total Fe (%)	43	16	5	20	15

* The A–E doublets are indentified in Fig. 5.

CATION DISTRIBUTION IN SURINAMITE, KHMARALITE, AND RELATED MINERALS

The present structure refinement of surinamite from "Christmas Point" not only confirms the tetrahedral ordering originally determined by Moore and Araki (1983), but also reconciles the X-ray unit-cell content with the analytical chemical composition and clarifies uncertainties regarding the cation ordering on the octahedral sites. Overall, the surinamite structure shows an essentially complete charge ordering on both the tetrahedral and octahedral sub-lattices. All site occupancies correlate well with the site volumes or the average bond distances (Table 3) and also yield uniform displacement parameters (U_{eq} in Table 4), as expected for a structure based on close packing with fully occupied cation sites. As discussed below, the ordered cation distribution in surinamite distinguishes it from other related minerals of the sapphirine-khmaralite series or

aenigmatite group.

The new refinement of the surinamite structure necessitates a readjustment in the interpretation of cation ordering in khmaralite. The new analysis (Table 1) and refinement of 2292C yields a Be/Si ratio 10% higher than that reported by Moore and Araki (1983), i.e., 0.340 vs. 0.309. The Be/Si ratio determined by Moore and Araki (1983) had been used to calibrate the ion microprobe data on khmaralite, and this Be content was used as input in the refinement (Barbier et al. 1999). Applying the new ratio to the ion probe data used by Barbier et al. (1999), the BeO content of type khmaralite increases to 2.77 wt% and the revised formula is $Ca_{0.04}Mg_{5.44}Fe^{3+}_{0.25}Fe^{2+}_{1.73}Al_{14.19}Be_{1.56}B_{0.02}Si_{4.77}O_{40}$. A refinement of khmaralite with an unconstrained Be content results in Be occupancies identical within 1% to those reported by Barbier et al. (1999) except Be occupancy of T3 increased from 18% to 20%. However, in view of the complexity of the khmaralite structure, the X-ray refinement is expected to be insensitive to a 10% increase in the Be content and a total Be + B content constrained to 1.58. We, therefore, can assume that the revised formula for khmaralite is valid.

In surinamite, Be is almost entirely sequestered at the most-polymerized, topologically unique, T1 tetrahedral site. This finding suggests an upper limit of 1 Be atom per formula unit (5 T sites, or 16 O atoms) for the surinamite structure. The cation ordering along the tetrahedral chain, viz., T1(Be)-T4(Si)-T5(Al)-T2(Si), and in the side branch, viz., T3(Si), is consistent with a driving force based on charge balance around the bridging oxygen atoms. For instance, the Be-rich T1 site and the Al-rich T5 site only share corners with the Si-rich T2, T3, and T4 sites (Fig. 2), thus avoiding unfavorable Be-O-Al linkages. The near complete Be ordering in surinamite contrasts with the partial ordering of Be in khmaralite, in which two of the six tetrahedral sites are topologically equivalent to the most-polymerized T site in surinamite (Barbier et al. 1999). As a result, Be ordering on a single site is not favored in spite of the Be content being only 0.78 Be per formula unit (6 T sites, or 20 O atoms). Because the two Be-bearing sites in sapphirine are adjacent to each other in the tetrahedral chain, the avoidance of Be-O-Be linkages leads to a maximum of 1 Be per formula unit as indicated by a recent study of synthetic beryllian sapphirines (Christy et al. 2000, and Christy et al. in preparation). The same conclusion also applies to the structures of Be-bearing minerals of the aenigmatite group, such as "makarochkinite" (Yakubovich et al. 1990; Barbier et al. 2001 and in preparation) and høgtuvaite (Grauch et al. 1994), which contain sapphirine-like tetrahedral chains. The different topologies of the tetrahedral chains in the surinamite and sapphirine structures account for the higher Be contents observed in surinamite relative to associated sapphirine/khmaralite at "Christmas Point" and "Zircon Point" in Antarctica (Grew 1981, 1998; Grew et al. 2000) or at South Harris in Scotland (Baba et al. 2000).

A tetrahedral cation distribution similar to that in natural surinamite is also present in the germanate surinamite analog, $^{VI}(Mg_4Ga_2)^{IV}(Ga_2Ge_3)O_{16}$ (Barbier 1998). In this case, the Ga-rich T1 site shares corners with the Ge-rich T2, T3, and T4 sites and the charge ordering along the tetrahedral chain is completed by the Ga-rich T5 site. However, the smaller charge difference between the Ga^{3+} and Ge^{4+} cations results in some significant Ga-Ge exchange on two of the sites. A similar tetrahedral ordering appears to be also present in the other surinamite analog, $^{VI}(Mg_4Al_2)^{IV}(Al_2Ge_3)O_{16}$, but a full structure refinement has so far been precluded by the presence of microscopic intergrowths of the *C*2/*c* and *P*2/*n* surinamite variants (Barbier 1996).

A last point of interest regarding the tetrahedral cation distribution in surinamite is the absence of tetrahedral Fe^{3+} as clearly established by the present X-ray and Mössbauer data. This result is consistent with the very minor amount of tetrahedral Fe^{3+} found by single-crystal refinement in khmaralite (2–3% Fe^{3+} in some of the T sites; Barbier et al. 1999) and with the absence of tetrahedral Fe^{3+} in Fe-rich serendibite (Grew et al. 1991; Van Derveer et al. 1993) and a terrestrial rhönite (Bonaccorsi et al. 1990), two minerals from the aenigmatite group with higher Fe^{3+}/Fe^{2+} ratios than surinamite. Given these findings, a combined crystallographic and Mössbauer spectroscopic study analogous to this one is necessary to clarify the distribution of Fe^{3+} in sapphirine. Taking the sapphirine and aenigmatite groups as a whole, one can propose that only in Al-poor phases, or in phases with insufficient Si + Al + Be + B contents, should tetrahedral Fe^{3+} be present in relatively large amounts (see also Kunzmann 1999). Such phases include Al-poor rhönites (Johnston and Stout 1985; Bonaccorsi et al. 1990), dorrite (Cosca et al. 1988), and the synthetic SFCA ferrite (Hamilton et al. 1989).

The octahedral cation distribution in surinamite is also ordered, at least in terms of a charge ordering among the divalent (Mg^{2+}, Fe^{2+}) and trivalent (Al^{3+}, Fe^{3+}) cations. As already noted, this ordering correlates well with the size of the octahedral sites (Table 3), which, in turn, reflect the pattern of edge sharing within the octahedral sub-lattice. For instance, the larger M^{2+} cations occupy the M1, M5, and M8 sites, which have fewer shared edges and, therefore, inherently larger volumes. On the other hand, the concentration of M^{2+} cations on the M7 site, in spite of a larger fraction of shared edges, corresponds to an M^{2+}/M^{3+} ordering within the (001) octahedral walls of the surinamite structure (Fig. 2). Similar octahedral ordering schemes are also found in the structures of the surinamite analogs (Barbier 1998), as well as in the related structures of sapphirine-2*M* (Higgins and Ribbe 1979), sapphirine-1*A* (Merlino 1980), and khmaralite (Barbier et al. 1999). The cation ordering in the aenigmatite-related structures of serendibite (Van Derveer et al. 1993), rhönite (Bonaccorsi et al. 1990), and "makarochkinite" (Yakubovich et al. 1990; Barbier et al. 2001) is also similar but less directly comparable to that in surinamite due to the particular crystal chemical role of the larger Na^{+} and Ca^{2+} cations.

The relatively high Fe content in surinamite is accommodated through extensive Mg-Fe^{2+} and Al-Fe^{3+} exchange only on the octahedral sites. The resulting Fe distribution and Fe^{2+}-Fe^{3+} ordering have been shown above to account well for the Mössbauer and optical absorption spectra. The octahedral Fe distribution is clearly not even: the high Fe^{2+} population of the M1 site alone accounts for about 38% of all Fe in surinamite (Table 3). The concentration of Fe on M1 can be understood in terms of the particular topology of that site, which allows it to accommodate the large Fe^{2+} cation. Not only is the site volume large due to the small number of shared edges, but the cation-

cation repulsions associated with edge-sharing between M1 and the M^{3+}-rich M6 and M9 sites (Fig. 2) can be relieved by substantial displacement of the M1 cation from the center. This is indicated by the distribution of M1-O bond distances, with three shorter and three longer bonds differing by about 0.2 Å, showing that the M1 cation is strongly displaced away from the shared edges (Table 6 and Fig. 2). The formation of particularly short M1-O11 and M1-O10 bonds (2.03 and 2.08 Å, respectively) is also consistent with bond-valence arguments: since the O10 and O11 atoms bridge the M1 site and the Be-rich T1 site (plus the T2 or T3 sites), shorter and stronger M1-O bonds can compensate for weaker Be-O bonds so as to maintain proper bond-valence sums around the bridging oxygen atoms. The resulting strong distortion of the M1 site may then also contribute to the strong partitioning of the Fe^{2+} cation in that site through electronic crystal-field effects.

An important implication of the revised Be content in khmaralite is the increase from 0.125 to 0.248 in the amount of Fe^{3+} calculated from stoichiometry. Based on refined site occupancies (Barbier et al. 1999), 0.18 of 0.27 Fe present on the Al-rich M sites is Fe^{3+}, and given the uncertainty associated with calculating Fe^{3+} from stoichiometry, it is possible that all 0.27 Fe on these sites is Fe^{3+}. The revised Fe^{3+} content is thus consistent with the presence on the octahedral sites of Al-Fe^{3+} mixing, rather than Al-Fe^{2+} mixing as has been shown above to be the case in surinamite.

In summary, the ordered cation distributions on the tetrahedral and octahedral sub-lattices of the surinamite structure are complementary to each other and result, in particular, in an Fe-Be clustering in the M1-T1 sites. Interestingly, a similar clustering has also been observed on the equivalent sites of the khmaralite structure, but to a lesser degree consistent with the less-pronounced ordering of tetrahedrally coordinated cations in that structure (Barbier et al. 1999).

ACKNOWLEDGMENTS

This work was supported by research grants from the Natural Sciences and Engineering Research Council of Canada to J.B. and from the U.S. National Science Foundation grant OPP-0087235 to E.S.G. Financial support from the Swedish Natural Science Research Council (NFR) is greatly appreciated by U.H. The single-crystal X-ray data were collected by J. Britten in the Chemistry Department at McMaster University. We thank the Australian National Antarctic Research Expedition and the Japanese Antarctic Research Expedition for providing the logistics support necessary for collecting samples 2292C and EG99012207. Constructive reviews of this manuscript by G. Rossman and M. Darby Dyar are greatly appreciated. The MSA color fund supported Fig. 1; tax-deductible contributions welcome.

REFERENCES CITED

Amthauer, G. and Rossman, G.R. (1984) Mixed valence of iron in minerals with cation clusters. Physics and Chemistry of Minerals, 11, 37–51.

Araki, T. and Zoltai, T. (1972) Crystal structure of babingtonite. Zeitschrift für Kristallographie, 135, 355–373.

Armbruster, T. and Oberhänsli, R. (1988) Crystal chemistry of double-ring silicates. Structural, chemical and optical variation in osumilites. American Mineralogist, 73, 585–594.

Baba, S, Grew, E.S., Shearer, C.K., and Sheraton, J.W. (2000) Surinamite, a high-temperature metamorphic beryllosilicate from Lewisian sapphirine-bearing kyanite-orthopyroxene-quartz-potassium feldspar gneiss at South Harris, N.W. Scotland. American Mineralogist, 85, 1474–1484.

Barbier, J. (1996) Surinamite analogs in the MgO-Ga_2O_3-GeO_2 and MgO-Al_2O_3-GeO_2 systems. Physics and Chemistry of Minerals, 23, 151–156.

———(1998) Crystal structures of sapphirine and surinamite analogues in the MgO-Ga_2O_3-GeO_2 system. European Journal of Mineralogy, 10, 1283–1293.

Barbier, J., Grew, E.S., Moore, P.B., and Su, S-C. (1999) Khmaralite, a new beryllium-bearing mineral related to sapphirine: A superstructure resulting from partial ordering of Be, Al and Si on tetrahedral sites. American Mineralogist, 84, 1650–1660.

Barbier, J., Grew, E.S., Yates, M.G., and Shearer, C.K. (2001) Beryllium minerals related to aenigmatite. Geological Association of Canada, Mineralogical Association of Canada, Canada Geophysical Union, Joint Annual Meeting, Abstracts Volume, 26, 7.

Bonaccorsi, E., Merlino, S., and Pasero, M. (1990) Rhönite: structural and microstructural features, crystal chemistry and polysomatic relationships. European Journal of Mineralogy, 2, 203–218.

Burns, R.G. (1993) Mineralogical Applications of Crystal Field Theory. In A. Putnis and R.C. Lieberman, Eds., Cambridge Topics in Mineral Physics and Chemistry 5, p. 551. Cambridge University Press, 2nd ed., U.K.

Burns, R.G. and Dyar, M.D. (1991) Crystal chemistry and Mössbauer spectra of babingtonite. American Mineralogist, 76, 890–899.

Burns, R.G. and Solberg, T.C. (1990) ^{57}Fe-bearing oxide, silicate, and aluminosilicate minerals. In L.M. Coyne, S.W.S. McKeever, and D.F. Blake, Eds., Spectroscopic Characterization of Minerals and Their Surfaces, p. 262–283. American Chemical Society Symposium Series 415, Washington, D.C.

Cawthorn, R.G. and Collerson, K.D. (1974) The recalculation of pyroxene end-member parameters and the estimation of ferrous and ferric iron content from electron microprobe analyses. American Mineralogist, 59, 1203–1208.

Christy, A.G. and Putnis, A. (1988) Planar and line defects in the sapphirine polytypes. Physics and Chemistry of Minerals, 15, 548–558.

Christy, A.G., Tabira, Y., Hölscher, A., Grew, E.S., and Schreyer, W. (2000) Synthetic beryllian sapphirine: Structural characterization. Geological Society of America Abstracts with Programs, 32(7), A-54.

Coey, J.M.D. (1984) Mössbauer spectroscopy of silicate minerals. In G.J. Long, Ed., Mössbauer Spectroscopy Applied to Inorganic Chemistry, p. 443–509. Plenum Press, New York.

Cosca, M.A., Rouse, R.C., and Essene, E.J. (1988) Dorrite [$Ca_2Mg_2Fe^{3+}_4Si_2Al_4O_{20}$], a new member of the aenigmatite group from a pyrometamorphic melt-rock. American Mineralogist, 73, 1440–1448.

de Roever, E.M.F., Kieft, C., Murray, E., Klein, E., and Drucker, W.H. (1976) Surinamite, a new Mg-Al silicate from the Bakhuis Mountains, western Surinam. I. Description, occurrence, and conditions of formation. American Mineralogist, 61, 193–197.

de Roever, E.M.F., Lattard, D., and Schreyer, W. (1981) Surinamite: a beryllium-bearing mineral. Contributions to Mineralogy and Petrology, 76, 472–473.

Ericsson, T.L. and Wäppling, R. (1976) Texture effects in 3/2-1/2 Mössbauer spectra. Journal de Physique, Colloque C6, supplément no. 12, 719–723.

Geiger, C.A., Armbruster, T., Khomenkov, V., and Quartier, S. (2000) Cordierite I: The coordination of Fe^{2+}. American Mineralogist, 85, 1255–1264.

Goldman, D.S. and Rossman, R.G. (1978) The site distribution of iron and anomalous biaxiality in osumilite. American Mineralogist, 63, 490–498.

Goldman, D.S., Rossman, R.G., and Dollase, W.A. (1977) Channel constituents in cordierite. American Mineralogist, 62, 1144–1157.

Grauch, R.I., Lindahl, I., Evans, H.T. Jr., Burt, D.M., Fitzpatrick, J.J., Foord, E.E., Graff, P-R., and Hysingjord, J. (1994) Høgtuvaite, a new beryllian member of the aenigmatite group from Norway, with new X-ray data on aenigmatite. The Canadian Mineralogist, 32, 439–448.

Grew, E.S. (1981) Surinamite, taaffeite and beryllian sapphirine from pegmatites in granulite-facies rocks of Casey Bay, Enderby Land, Antarctica. American Mineralogist, 66, 1022–1033.

———(1998) Boron and beryllium minerals in granulite-facies pegmatites and implications of beryllium pegmatites for the origin and evolution of the Archean Napier Complex of East Antarctica. Memoirs of the National Institute of Polar Research, Special Issue, 53, 74–92.

Grew, E.S., Pertsev, N.N., Boronikhin, V.A., Borisosvkiy, S. Ye., Gates, M.G., and Marquez, N. (1991) Serendibite in the Tayozhnoye deposit of the Aldan Shield, eastern Siberia, USSR. American Mineralogist, 76, 1061–1080.

Grew, E.S., Yates, M.G., Barbier, J., Shearer, C.K., Sheraton, J.W., Shiraishi. K., and Motoyoshi, Y. (2000) Granulite-facies beryllium pegmatites in the Napier Complex in Khmara and Amundsen Bays, western Enderby Land, East Antarctica. Polar Geoscience, 13, 1–40.

Hamilton, J.D.G., Hoskins, B.F., Mumme, W.G., Borbidge, W.E., and Montague, M.A. (1989) The crystal structure and crystal chemistry of $Ca_{2.3}Mg_{0.8}Al_{1.5}Si_{1.1}Fe_{8.3}O_{20}$ (SFCA): solid solution limits and selected phase relationships of SFCA in the SiO_2-Fe_2O_3-CaO(-Al_2O_3) system. Neues Jahrbuch für Mineralogie Abhandlungen, 161, 1–26.

Higgins, J.B. and Ribbe, P.H. (1979) Sapphirine II: A neutron and X-ray diffraction study of $(Mg\text{-}Al)^{VI}$ and $(Si\text{-}Al)^{IV}$ ordering in monoclinic sapphirine. Contributions to Mineralogy and Petrology, 68, 357–368.

Hölscher, A., Schreyer, W., and Lattard, D. (1986) High-pressure, high-temperature stability of surinamite in the system MgO-BeO-Al_2O_3-SiO_2-H_2O. Contributions to Mineralogy and Petrology, 92, 113–127.

Ingalls, R. (1964) Electric-field gradient tensor in ferrous compounds. Physical Review 133, 3A, A787–A795.

Jernberg, P. and Sundqvist, B. (1983) A versatile Mössbauer analysis program. Uppsala University, Institute of Physics (UUIP-1090).

Johnston, A.D. and Stout, J.H. (1985) Compositional variation of naturally occurring rhoenite. American Mineralogist, 70, 1211–1216.

Koch-Müller, M., Kahlenberg, V., Schmidt, C., and Wirth, R. (2000) Location of OH groups and oxidation processes in triclinic chloritoid. Physics and Chemistry of Minerals, 27, 703–712.

Kunzmann, T. (1999) The aenigmatite-rhönite mineral group. European Journal of Mineralogy, 11, 743–756.

Mattson, S.M. and Rossman, G.R. (1987a) Identifying characteristics of charge transfer transitions in minerals. Physics and Chemistry of Minerals, 14, 94–99.

———(1987b) Fe^{2+}-Fe^{3+} interactions in tourmaline. Physics and Chemistry of Minerals, 14, 163–171.

Merlino, S. (1980) Crystal structure of sapphirine-1*Tc*. Zeitschrift für Kristallographie, 151, 91–100.

Moore, P.B. and Araki, T. (1983) Surinamite, *ca*. $Mg_3Al_4Si_3BeO_{16}$: its crystal structure and relation to sapphirine *ca*. $Mg_{2.8}Al_{7.2}Si_{1.2}O_{16}$. American Mineralogist, 68, 804–810.

Robinson, K., Gibbs, G.V., and Ribbe, P.H. (1971) Quadratic elongation: a quantitative measure of distortion in coordination polyhedra. Science, 172, 567–571.

Sheldrick, G.M. (1993) SHELXL93, program for the refinement of crystal structures. University of Göttingen, Germany.

———(1996) SADABS, Siemens area detector absorption correction software. University of Göttingen, Germany.

Shen, G., Fei, Y., Hålenius, U., and Wang, Y. (1994) Optical absorption spectra of $(Mg,Fe)SiO_3$ silicate perovskites. Physics and Chemistry of Minerals, 20, 478–482.

Smith, G. and Strens, R.G.J. (1976) Intervalence transfer absorption in some silicate, oxide and phosphate minerals. In R.G.J. Strens, Ed., The Physics of Minerals and Rocks, p. 583–612. Wiley, New York.

Steffen, G., Seifert, F., and Amthauer, G. (1984) Ferric iron in sapphirine: a Mössbauer spectroscopic study. American Mineralogist, 69, 339–348.

Tang Kai, A., Annersten, H., and Ericsson, T. (1980) Molecular orbital (MSXα) calculations of s-electron densities of tetrahedrally coordinated ferric iron: Comparison with experimental isomer shifts. Physics and Chemistry of Minerals, 5, 343–349.

Van Derveer, D.G., Swihart, G.H., Sen Gupta, P.K., and Grew, E.S. (1993) Cation occupancies in serendibite: a crystal structure study. American Mineralogist, 78, 195–203.

Woodland, A.B. and O'Neill, H.St.C. (1993) Synthesis and stability of $Fe^{2+}_{3}Fe^{3+}_{2}Si_3O_{12}$ garnet and phase relations with $Fe_3Al_2Si_3O_{12}$-$Fe^{2+}_{3}Fe^{3+}_{2}Si_3O_{12}$ solutions. American Mineralogist, 78, 1002–1015.

Yakubovich, O.V., Malinovskii, Yu. A., and Polyakov, V.O. (1990) Crystal structure of makarochkinite. Soviet Physics Crystallography, 35, 818–822.

MANUSCRIPT RECEIVED MAY 17, 2001
MANUSCRIPT ACCEPTED NOVEMBER 29, 2001
MANUSCRIPT HANDLED BY BARB DUTROW